Natural convection in vertical, parallel-plate channels with appended unheated entrances

A. Campo
Department of Mechanical Engineering, The University of Vermont, Burlington, Vermont, USA
O. Manca and B. Morrone
Dipartimento di Ingegneria Aerospaziale e Meccanica, Seconda Università degli studi di Napoli, via Roma, Aversa (CE), Italy

Received April 2002
Revised January 2004
Accepted February 2004

Abstract

Purpose – To address the impact of adding insulated plate extensions at the entrance of an isoflux vertical parallel-plate channel on the thermal performances of natural convection in air for these systems.

Design/methodology/approach – The model relies on the full elliptic conservation equations which are solved numerically in a composite three-part computational domain by means of the finite-volume method.

Findings – Results are reported in terms of wall temperatures, induced mass flow rates, as well as velocity and temperature profiles of the air for various thermal and geometric parameters. The wall temperatures increase when the extensions are appended at the inlet of the channel. Wall temperature profiles strongly depend on the Rayleigh number and the dependence of the heated channel aspect ratio is weaker than the extension ratio. Velocity and temperature profiles modify inside the heated channel due to the thermal development. In addition, correlation equations for main engineering quantities, such as the induced mass flow rate, average Nusselt number and dimensionless maximum wall temperature in terms of the channel Rayleigh number, channel aspect ratio and extension ratio are presented.

Research limitations/implications – The investigation has been carried out in the following ranges: 10^3-10^5 for the Rayleigh number, 5.0-15.0 for the channel aspect ratio and 1.0-5.0 for the extension ratio. The hypotheses on which the present analysis is based are: two-dimensional, laminar and steady-state flow, constant thermophysical properties with the Boussinesq approximation.

Practical implications – Thermal design of heating systems in manufacturing processes, evaluation of heat convective coefficients and maximum attained wall temperatures.

Originality/value – Evaluation of the thermal and velocity fields and correlation equations for the Nusselt number and maximum dimensionless temperatures in natural convection in air for vertical channels. The paper is useful to thermal designers.

Keywords Convection, Channel flow, Heat transfer, Correlation analysis

Paper type Research paper

International Journal for Numerical Methods in Heat & Fluid Flow
Vol. 15 No. 2, 2005
pp. 183-204

0961-5539
DOI 10.1108/09615530510578447

This study was supported by the MURST with a 2001 grant Research Program and the CNR with a grant on Bilateral Research Project n.99.03198.07.

Nomenclature

a = thermal diffusivity, m^2/s
b = channel gap, m
g = gravity acceleration, m/s^2
Gr = Grashof number, equation (6)
k = thermal conductivity, W/mK
L = height of heated plate, m
L_{ext} = height of insulated plate extension, m
L_{tot} = height of total channel, $L + L_{ext}$, m,
L_x = height of reservoir, m
L_y = width of reservoir, m
Nu = average Nusselt number, equation (8)
n_X, n_Y = grid nodes along X, Y
p = pressure, Pa
P = dimensionless pressure, equation (5)
Pr = Prandtl number, equation (6)
q_w = uniform wall heat flux, W/m^2
r^2 = regression coefficient
Ra = Rayleigh number, equation (6)
Ra* = channel Rayleigh number, Ra b/L
t = time, s
T = temperature, K
u, v = velocity components along x, y, m/s
U, V = dimensionless velocities, equation (5)
x, y = Cartesian coordinates, m
X, Y = dimensionless coordinates, equation (5)

Greek symbols

β = volumetric coefficient of expansion, 1/K
θ = dimensionless temperature, equation (5)
ν = kinematic viscosity, m^2/s
ψ = stream function, m^2/s
Ψ = dimensionless stream function, equation (5)
ρ = density, kg/m^3
ω = vorticity, 1/s
Ω = dimensionless vorticity, equation (5)

Subscripts

Asymp = asymptotic value
b = bulk
max = maximum value
0 = bare channel
w = wall
w_1 = left wall
w_2 = right wall
∞ = free stream condition

Introduction

Natural convection flows through vertical parallel-plate channels is a topic of continuing interest in several branches of engineering, such as natural ventilation, electronics cooling, heat exchange devices, etc. Since these channels are usually open to ambient conditions at both entrance and exit sections, natural convection is the most used economic technique for cooling. Further, natural convection is an attractive mode of cooling where reliability and low noise become paramount design considerations. These features have motivated a substantial body of research on natural convection in vertical parallel-plate channels but, as will be discussed shortly, numerous important issues remain unresolved.

To design a cooling channel properly the design engineer needs to know the magnitude of the convective heat transfer coefficient associated with the working fluid either from theoretical, numerical, or experimental analyzes. In general, heat transfer rates associated with natural convection flows in channels are low compared to equivalent situations involving forced convection. From the standpoint of engineering design, this singular feature constitutes an important lower bound for the heat removal capabilities of these channels.

Aihara (1973) was the first investigator who treated the inflow boundary condition at the entrance of a vertical channel to be used in the simplified parabolic model

of the conservation equations. His findings provided a first-order approximation for the pressure drop inside the channel due to fluid acceleration.

The vast majority of the analytic studies on natural convection between parallel-plate vertical channels have employed a two-dimensional parabolic model connected to a computational domain that is coincident with the physical domain. Such a model/domain assembly takes no cognizance of the intricacies of the inflow and outflow boundary conditions attached to the channel. The leading works on the modelling of natural convection flows through vertical parallel-plate channels heated symmetrically utilizing the full elliptic equations coupled with an enlarged computational domain are those of Chang and Lin (1989, 1990), Kettleborough (1972), Manca *et al.* (1994), Martin *et al.* (1991), Morrone *et al.* (1997), Nakamura *et al.* (1982), Naylor *et al.* (1991), Ramanahtan and Kumar (1991) and Shyy *et al.* (1992) as recently reviewed by Manca *et al.* (2000).

The use of enhancement techniques is a commonly accepted design principle for forced convection heat transfer in ducts (Bergles, 1998; Webb, 1994). Such techniques may involve the use of extended surfaces, roughness elements, surface interruptions, twisted tapes, etc. In general, the heat transfer enhancement is accomplished by the modification of the pattern of the forced flow, so that the increased heat transfer capability is generally accompanied by a penalty in pressure drop. A rational basis for assessing the benefits of the heat transfer enhancement taking into account the pressure drop has been discussed at length by Bergles (1998) and Webb (1994). The central point of the foregoing discussion is that in those forced convection ducts where the flow rate can be varied independently, trade-offs can be made between the magnitude of the heat transfer and the magnitude of the pressure drop. This capability greatly enlarges the spectrum of possibilities for attaining a desired design goal subject to given constraints. In contrast, Sparrow *et al.* (1980) have written that in a natural convection situation, the rate of fluid flow through a vertical, parallel-plate channel cannot be independently controlled. Rather, the flow rate is established by a dynamic balance between the buoyancy forces and the friction forces. Thus, in an enhanced natural convection channel, the flow rate cannot be independently adjusted to achieve some desired relationship with an un-enhanced channel. In reality, the channel adjusts itself in accordance with the changes that have occurred in buoyancy and friction as a result of the implementation of the augmented technique. The absence of an independent control of the flow rate in natural convection removes some of the flexibilities which may enable the fulfillment of specific performance goals in forced convection. On the other hand, the concerns about pressure drops that are inherent in forced convection are irrelevant in natural convection because no pump or blower is needed for the latter. Therefore, the evaluation of an enhancement technique in natural convection may be based on heat transfer performance strictly, without concern about the fluid flow issues. Consequently, although there are fewer design options in natural convection enhancement than in forced convection enhancement, the design goals and constraints are fewer and simpler.

It is noteworthy that in the extensive literature on heat transfer enhancement there is little work on natural convection, refer, for example, Raithby and Hollands (1998) and Webb (1994). In this regard, the enhancement technique to be investigated here is the attachment of unheated plates at the entrance of heated vertical parallel-plate channels. Two papers have been found in the specialized literature which are devoted to this specific topic. Wirtz and Haag (1985) reported

experimental measurements for symmetric isothermal heated vertical plates. Lee (1994) conducted a theoretical study with isothermal and isoflux plates conforming a channel. A drawback of the numerical work of the latter is that the conservation equations were modelled in parabolic form using Aihara's inflow boundary condition in a computational domain that matches the physical domain. Since no comparisons were made with the experimental data the validity of the simplified model is questionable. Instead, in Campo *et al.* (1999) the full elliptic conservation equations were solved in a composite computational domain and discrepancies were found with Lee (1994), especially at low Rayleigh numbers.

From a framework of heat transfer enhancement, it is necessary to study the decisive role played by the addition of two colinear insulated plates to the entry of a vertical parallel-plate channel from a broader perspective. This aspect constitutes the central motivation for undertaking this project. Chang and Lin (1989, 1990), Kettleborough (1972), Manca *et al.* (1994), Martin *et al.* (1991), Morrone *et al.* (1997), Nakamura *et al.* (1982), Naylor *et al.* (1991), Ramanahtan and Kumar (1991) and Shyy *et al.* (1992) have delineated the pressing importance of the elliptic model for the conservation equations in conjunction with the physical domain and two extended computational domains. Accordingly, an elliptic model was preferred here to analyze the heat and fluid flow inside a vertical, parallel-plate channel with symmetric heating conditions. The computational domain having an I-shape comprises the actual physical domain between the two insulated/heated channel plates and two relatively large domains placed at the channel entrance and at the channel exit. The added artificial domains seek to resemble open spaces that serve to accommodate the diffusion phenomena by momentum and energy that could occur in the fluid flow in the vicinity of the channel. The conservation equations have been solved by the finite-volume discretization technique providing the velocity, pressure and temperature fields of the fluid medium and the temperature profiles of the heated walls.

Analysis and numerical solution method

The physical system under study is made of a vertical, parallel-plate channel. The two heated plates are at uniform heat flux q_w and insulated plate extensions are placed upstream of the heated plates. The system, shown in Figure 1(a), is characterized by the height of the heated plate L, the channel gap b, the height of the upstream insulated plate extension L_{ext} and the total height L_{tot}. The main geometrical ratios employed in the analysis are: L/b, the channel aspect ratio, L_{ext}/L, the insulated extension ratio, and L_{tot}/L, the total extension ratio. Buoyant air at atmospheric conditions moves up through the channel gap cooling the heated plates.

Under steady-state conditions, the two-dimensional conservation equations for a fluid with Boussinesq approximation are:

$$\frac{\partial(u\omega)}{\partial x} + \frac{\partial(v\omega)}{\partial y} = \nu\nabla^2\omega - g\beta\frac{\partial T}{\partial y} \tag{1}$$

$$\frac{\partial^2\psi}{\partial x^2} + \frac{\partial^2\psi}{\partial y^2} = -\omega \tag{2}$$

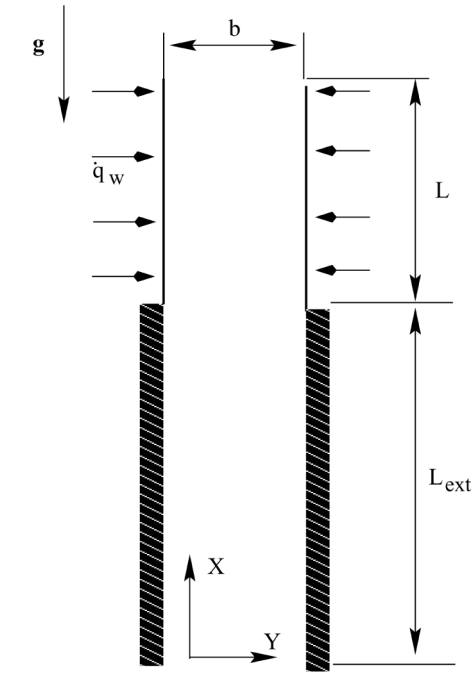

(a)

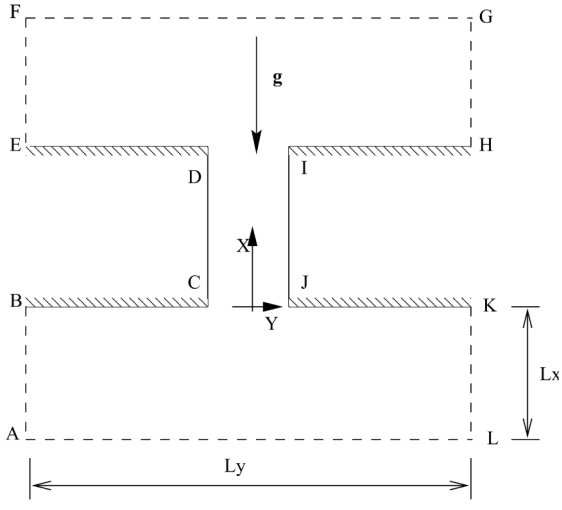

(b)

Figure 1.
(a) Channel with unheated entrance; and
(b) computational domain

$$\frac{\partial(uT)}{\partial x}+\frac{\partial(vT)}{\partial y}=a\nabla^2 T+\beta T\frac{Dp}{Dt} \tag{3}$$

In the preceding equations, the stream function is obtained by:

$$\frac{\partial\psi}{\partial y}=u;\quad \frac{\partial\psi}{\partial x}=-v$$

and the vorticity is:

$$\omega=\frac{\partial v}{\partial x}-\frac{\partial u}{\partial y}$$

respectively. It should be added that in equation (3) the material derivative of pressure has been neglected in the present analysis with respect to the temperature gradients (Gebhart *et al.*, 1988).

Following the recommendations of Campo *et al.* (1996) and Manca *et al.* (1994), an enlarged computational domain of finite extension, as shown in Figure 1(b), has been employed in this investigation to mimic the free-stream conditions of the air flow far away from the region of thermal disturbance induced by the heated plates.

In reference to Figure 1(b), the imposed boundary conditions can be written in abbreviated form as follows:

$$\begin{aligned}
&\frac{\partial\psi}{\partial y}=0,\quad \frac{\partial\omega}{\partial y}=0,\quad T=0 \quad \text{at AB and KL}\\
&\frac{\partial\psi}{\partial x}=0,\quad \frac{\partial\omega}{\partial x}=0,\quad T=0 \ \text{at} \quad \text{AL}\\
&\psi=\psi_{w1},\quad \frac{\partial\psi}{\partial x}=0,\quad \frac{\partial T}{\partial x}=0 \quad \text{at BC and DE}\\
&\psi=\psi_{w1},\quad \frac{\partial\psi}{\partial y}=0,\quad -k\frac{\partial T}{\partial y}=\left\{\begin{array}{ll} q_w & \text{heated part}\\ 0 & \text{unheated part}\end{array}\right\} \text{at CD}\\
&\psi=\psi_{w2},\quad \frac{\partial\psi}{\partial y}=0,\quad k\frac{\partial T}{\partial y}=\left\{\begin{array}{ll} q_w & \text{heated part}\\ 0 & \text{unheated part}\end{array}\right\} \text{at IJ}\\
&\frac{\partial^2\psi}{\partial y^2}=0,\quad \frac{\partial\omega}{\partial y}=0,\quad \frac{\partial T}{\partial y}=0 \quad \text{at EF and GH}\\
&\psi=\psi_{w2},\quad \frac{\partial\psi}{\partial x}=0,\quad \frac{\partial T}{\partial x}=0 \quad \text{at HI and JK}\\
&\frac{\partial^2\psi}{\partial x^2}=0,\quad \frac{\partial\omega}{\partial x}=0,\quad \frac{\partial T}{\partial x}=0 \quad \text{at FG}
\end{aligned} \tag{4}$$

The choice of the dimensionless variables:

$$X = \frac{x}{b}, \quad Y = \frac{y}{b}, \quad U = \frac{ub}{\nu}, \quad V = \frac{vb}{\nu}, \quad P = \frac{(p - p_\infty)b^2}{\rho\nu^2}, \quad \Psi = \frac{\psi}{\nu}, \quad \Omega = \frac{\omega b^2}{\nu}, \quad \theta = \frac{k(T - T_\infty)}{q_w b} \tag{5}$$

give way to the controlling dimensionless groups

$$\frac{L}{b}, \quad \frac{L_{tot}}{L}, \quad \mathrm{Gr} = \frac{g\beta q_w b^4}{k\nu^2}, \quad \mathrm{Pr} = \frac{\nu}{a}, \quad \mathrm{Ra} = \mathrm{Gr}\,\mathrm{Pr} \tag{6}$$

The channel aspect ratio L/b and the Rayleigh number Ra are commonly encapsulated into a dimensionless group $\mathrm{Ra}^* = \mathrm{Ra}\ b/L$ called the channel Rayleigh number.

An essential quantity to be evaluated in the calculations is the induced flow rate between the parallel plates which, in dimensionless terms, is:

$$\Psi_{w2} - \Psi_{w1} = \Delta\Psi = \int_0^1 U\,\mathrm{d}Y \tag{7}$$

Another main heat transfer quantity of interest is the average Nusselt number over the heated part of the plates channel, which relying on the dimensionless variables, is defined as:

$$\mathrm{Nu} = \frac{b}{L}\int_{L_{ext}/b}^{(L_{ext}+L)/b} \frac{\mathrm{d}X}{\theta_w(X)} \tag{8}$$

The numerical computations have been carried out by means of the control volume method. The vorticity and energy equations, equations (1) and (3), have been solved by implementing the alternating direction implicit (ADI) method with the false transient procedure (Roache, 1972). The second upwind scheme, recommended by Torrance (1985) has been employed to discretize the convective derivatives, while a classical three-point central scheme has been adopted for the diffusive derivatives. The convective terms were linearized following the iterative procedure suggested by Roache (1972). The stream function has been determined by the successive line overrelaxation (SLOR) method with an optimum relaxation factor of about 1.7. Once the equations of vorticity, stream function and energy have been solved, then the convergence criteria for the time-like step have to be checked. The steady-state-like condition attained was considered when the percentage variation of Ψ, Ω and θ was less than 10^{-5}.

The computational procedure was implemented by guessing an initial value for the stream functions ψ_{w2} at the right wall 2, and $\psi_{w1} = 0$, at the left wall 1. The selected value of the mass flow rate is verified on a global basis by integrating the momentum equation along the centerline of the vertical, parallel-plate channel in the chosen computational domain, as reported in detail by Morrone *et al.* (1997).

The discontinuity of the heat flux has been implemented by setting to zero the value of the heat flux at the insulated walls. Numerically this goal has been accomplished by evaluating the energy balance at the wall volumes with the boundary surface facing the plate set either insulated (i.e. heat flux equal to zero) or with imposed heat flux.

The analysis of the convergence of the code has been carried out by employing the Richardson extrapolation (Roache, 1998). The verification of the solutions is obtained by considering two different meshes, usually obtained by halving the mesh size. Indicating the coarse mesh solution with f_1 and the fine mesh solution with f_2, the Richardson extrapolation gives the asymptotic value of the function f evaluated at the same point in the two mesh systems:

$$f_{\text{asympt}} \cong \frac{4}{3} f_2 - \frac{1}{3} f_1$$

Applying this procedure to the base channel, the numerical experiments indicated that a grid consisting of $n_X = 71$ and $n_Y = 21$ nodes inside the channel furnished satisfactory results for aspect ratio L/b between 5 and 15. In Table I the induced flow rate is reported at $\text{Ra}^* = 10^3$ and $L/b = 10$ as function of the grid size; in the same table the percentage discrepancy between the actual value and the asymptotic one are shown. The discrepancies between this solution mesh system and the asymptotic values were about 1.5 per cent for the induced mass flow rate and less than 3 per cent for the average Nusselt number. These grid distributions guaranteed a global energy balance inside the channel with an accuracy of about 0.5 per cent. Both local and global mass conservation have also been checked and discrepancies of order 10^{-4} between the inflow and outflow mass flow rates were found.

Depending on the Rayleigh number and the selected aspect ratio, the vertical dimension of the reservoirs, L_x, ranged from one to two times the height of the channel, L, whereas the horizontal dimension of the reservoirs, L_y, was enlarged between 11 and 15 times the plate separation b.

The numerical procedure has been validated with available numerical and experimental results in Manca *et al.* (1994), producing satisfactory agreement. In addition, a comparison with some results of Lee (1994) has been carried out in Campo *et al.* (1999) giving good agreement.

Discussion of results

The present numerical investigation has been carried out with air ($\text{Pr} = 0.71$) as working fluid. The heat transfer and flow characteristics of air are obtained in terms of velocity and temperature fields for several thermal and geometrical configurations. With this information, design parameters of remarkable importance in industry such as the maximum wall temperatures (a local quantity) and the induced mass flow rates (a global quantity) are computed. The two sets of results involve the ratio between the actual quantity and the associated quantity for the "base case". The latter refers to the simple channel without insulated extension plates ($L_{\text{ext}}/L = 0$).

Table I.
Evaluation of induced mass flow rate number for the base case at $\text{Ra}^* = 10^3$ and $L/b = 10$ as function of the grid size

$n_X \times n_Y$	$\Delta\Psi$	Δ per cent
35×11	102.8	2.0
71×21	102.0	1.3
143×41	101	0.3
Asymptotic value	100.7	0.0

First, the wall temperature profiles, $\theta_w(X)$, are presented as function of the Ra* number, the channel aspect ratio L/b and the total extension ratio $L_{tot}/L = L_{ext}/L + 1$. Figure 2 shows the wall temperature profiles as function of the X coordinate along the wall at Ra* $= 10^3$ for channel aspect ratio equal to 5.0, 10 and 15 and several L_{tot}/L values, whereas the wall temperature profiles, θ_w, as function of X are reported for fixed channel aspect ratio $L/b = 10$ at Ra* $= 10^3$, 10^4 and 10^5 in Figure 3. The present results extend those presented in Campo *et al.* (1999) and this analysis focuses on the dependence on both the aspect ratio and the Rayleigh number.

The temperature profiles in the heated part of the channel in Figure 2 show an increment of their values along the wall for increasing L_{tot}/L at any L/b value. In addition, for any L/b value, the temperature profiles exhibit a steep derivative at the heated entrance region, which decreases with increasing X. The derivatives attain nearly a uniform value from some axial coordinate X onwards, whose value is based on the extension ratio L_{tot}/L. These X values are between 25 and 45 per cent of the heated plate height, with the lowest value being attained at $L_{tot}/L = 5.0$ and the highest at $L_{tot}/L = 1.0$. The shape of the profile is nearly linear and is as steeper as L_{tot}/L is higher. In addition, the temperature values are as high as L_{tot}/L. This situation is caused by the decrease of the induced mass flow rate which leads to a diminution of the heat transfer between the wall and the fluid. The increase of L_{tot}/L influences the maximum wall temperature value which is attained at lower X positions. In the down-flow region the wall exhibits slight greater temperature gradients the higher L_{tot}/L is, because of the edge effect. The wall temperatures are slight higher for the same L_{tot}/L with increasing L/b value.

The strong influence of the Rayleigh number, for fixed total aspect ratio, on the wall temperature profiles can be well observed in Figure 3, whereas the dependence of the temperatures on the L_{tot}/L ratio for fixed Ra* value decreases with increasing Ra*.

A good summary of what previously seen in Figures 2 and 3, is shown in Figure 4, which shows the variation of the maximum wall temperature ratios, $\theta_{w,max}/\theta_{w,max\,0}$, with the total extension ratio L_{tot}/L, for fixed Ra* $= 10^3$ (Figure 4(a)), and fixed L/b ratio, (Figure 4(b)).

The $\theta_{w,max\,0}$ represents the value of the maximum wall temperature for the base channel, for any Ra* and L/b values. It is clear that for any L/b value (Figure 4(a)) where the family of curves is parameterized by the aspect ratio L/b, $\theta_{w,max}/\theta_{w,max\,0}$ grows almost linearly with discrete increments of L_{tot}/L. Overall, the consecutive pair of curves for $L/b = 2.5$ and 5 and $L/b = 10$ and 15 exhibited imperceptible deviations among themselves. From a practical standpoint, it is important to recognize that huge increments of the wall temperature near the trailing edge of the heated plate $\theta_{w,max}/\theta_{w,max\,0}$ of about 35 per cent are achieved for the largest L_{tot}/L tested. In any case the difference between the values pertaining to $L_{tot}/L = 5.0$ is less than 3 per cent. This implies that it can be employed a system four times shorter for the same channel width, with a slight smaller dimensionless heating effect. This results in a marked reduction of the clearance. Anyway, if the dimensional channel width is fixed, for any Ra*, then the wall heat flux for $L/b = 10$ is four times that for the case with $L/b = 2.5$. The maximum wall temperature rise when $L/b = 10$ is four times that for $L/b = 2.5$. Despite that the temperature elevation of the directly heated plate is beneficial for heating purposes, care should be taken not to exceed the constrained design temperatures recommended by the manufacturer of the heater.

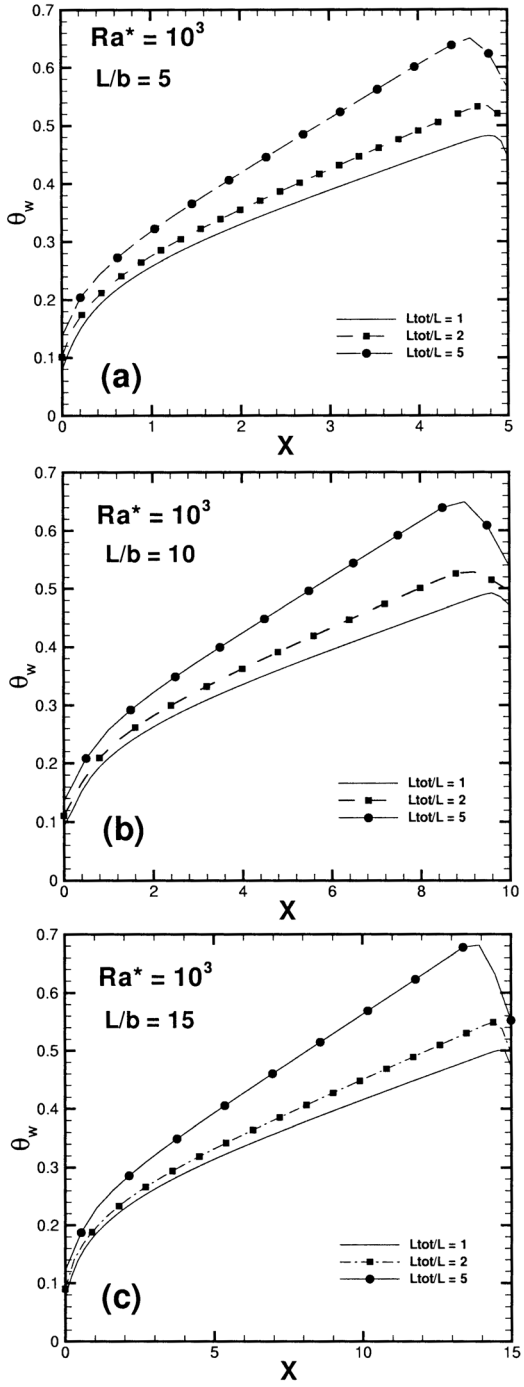

Figure 2.
Wall temperatures as a function of X for $Ra^* = 10^3$ and several L_{tot}/L: (a) L/b=5.0; (b) $L/b = 10.0$; and (c) $L/b = 15.0$

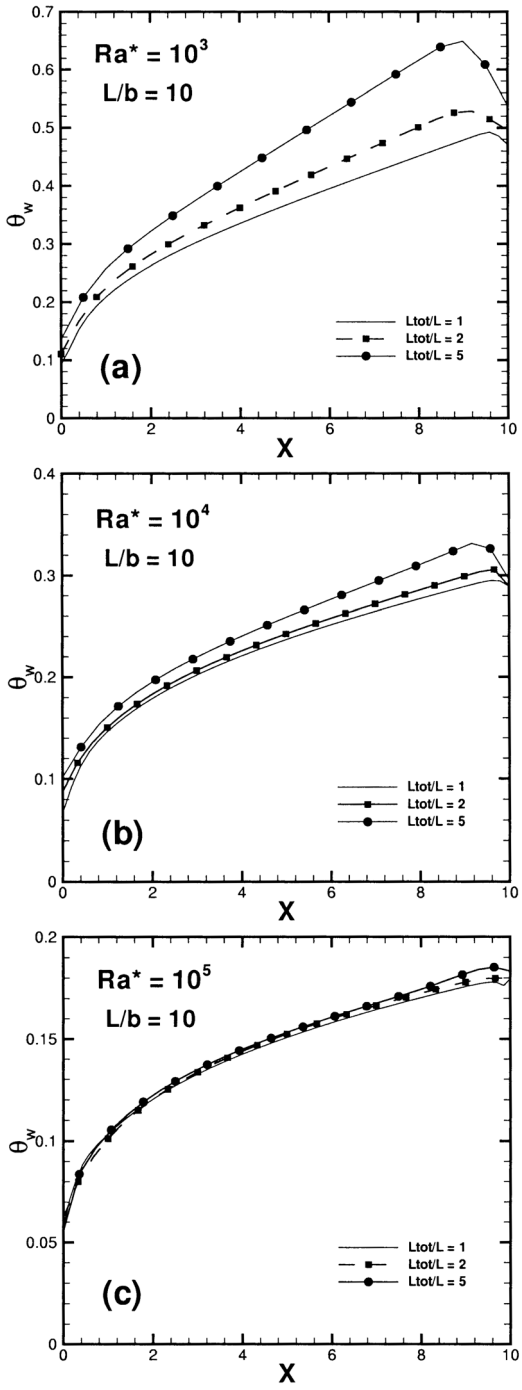

Figure 3.
Wall temperatures as a function of X for $L/b = 10$ and several L_{tot}/L: (a) $Ra^* = 10^3$; (b) $Ra^* = 10^4$; and (c) $Ra^* = 10^5$

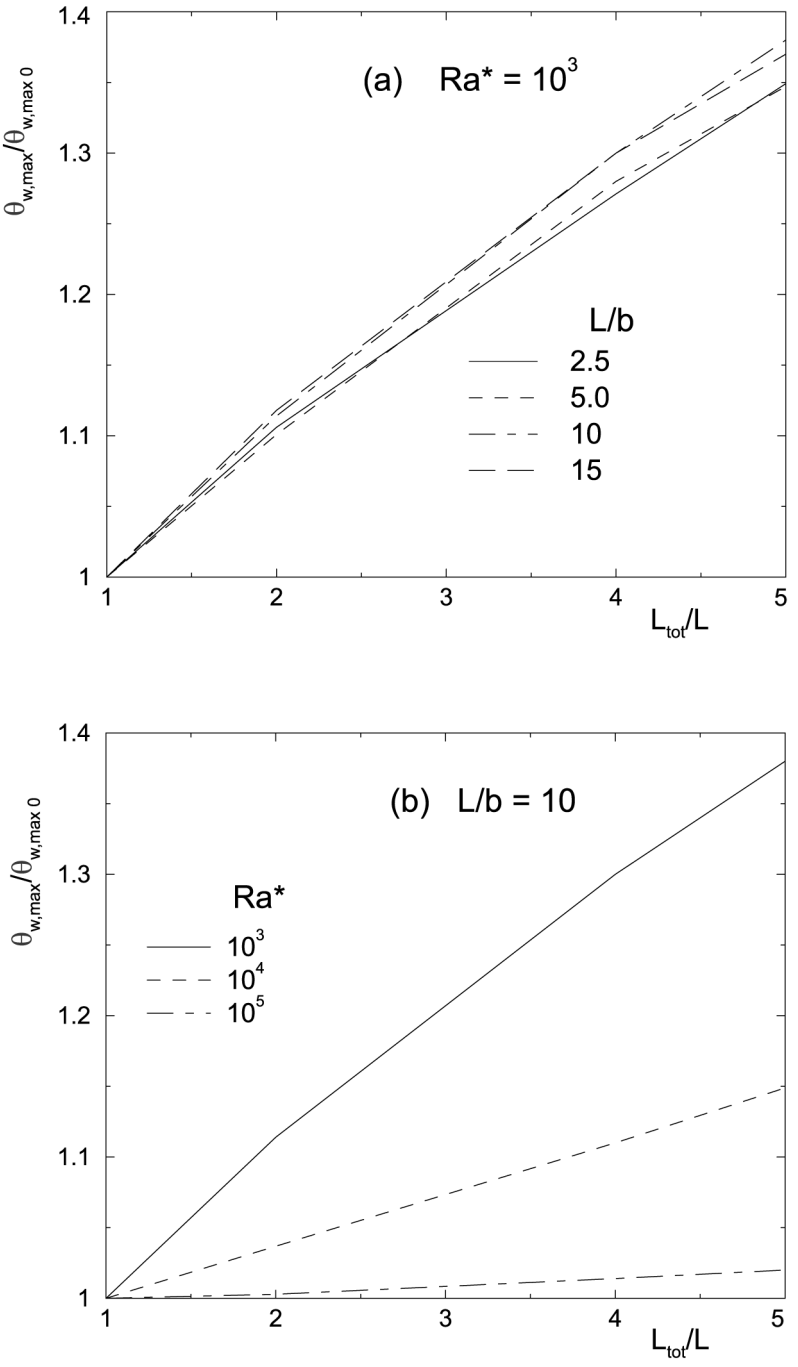

Figure 4.
Maximum wall temperature ratio as a function of L_{tot}/L for: (a) $Ra^* = 10^3$ and several L/b; and (b) $L/b = 10$ and several Ra^*

The impact of the total height ratio, L_{tot}/L, on the maximum wall temperature ratio, $\theta_{w,\,max}/\theta_{w,\,max\,0}$, for a fixed aspect ratio $L/b = 10$ and several Ra* values (10^3,10^4,10^5) is shown in Figure 4(b). The percentage increment of this ratio is more evident at the lowest Ra* value. In fact, the maximum percentage increment at $L_{tot}/L = 5.0$ correspond to 37 per cent, 15 per cent and about 2 per cent for Ra*=10^3, 10^4 and 10^5, respectively. This sequential behaviour is mainly due to the importance of the diffusive effects with respect to the convective ones. When the diffusion of momentum and energy are more important than the convection phenomenon (low Ra* numbers), then the presence of the insulated extensions upstream of the heated plates retards the induced flow rate. In fact, the increment of the wetted surface upstream of the heated zone induces greater pressure losses due to viscous effects. In other words, the longer the extensions the lower the induced flow rate. As a result, for $L_{tot}/L \rightarrow \infty$ the flow is no longer sucked from the bottom of the channel, since the heated part acts as a boundary effect. This pattern holds true for any Ra* values, but the flow rate reduction in the channel becomes more relevant for lower levels of Ra*.

In Table II the values of the induced mass flow rate and the maximum wall temperature for the base case are reported at $Ra^* = 10^3$ and the investigated L/b values, whereas in Table III the same quantities are reported for $L/b = 10$ and several Ra* values.

By fixing the channel aspect ratio, $L/b = 10$, and plotting the maximum wall temperature $\theta_{w,max}$ as function of Ra* for any L_{tot}/L values in Figure 5 the increment of L_{tot}/L brings a corresponding augmentation of $\theta_{w,max}$. Anyway, the $\theta_{w,max}$ values decrease with increasing Ra*, as expected. Increments of $\theta_{w,max}$ with L_{tot}/L of about 35 per cent are obtained for Ra* value of 10^3, whereas when Ra* is equal to 10^5 the difference is smaller than 3 per cent. When $L/b = 10$ by fixing the heat flux and comparing the case with $Ra^* = 10^3$ and 10^5, the channel width ratio is about 0.316 and a subsequent maximum wall temperature rise of about 1.17. That means the maximum dimensional wall temperature rise at $Ra^* = 10^3$ is 1.17 times that at $Ra^* = 10^5$. Instead, if one fixes the channel width, the wall heat flux ratio is 10^{-2} and the maximum dimensional wall temperature rise is about 3.7×10^{-2}. The same wall maximum dimensional temperature ratios for $Ra^* = 10^3$ and 10^4 are about 1.12 for fixed wall heat flux, and 0.20 for fixed channel width.

The values of the flow rate for the base case, $\Delta\Psi_0$, as function of the aspect ratio, L/b, are listed in Table II at $Ra^* = 10^3$ and for $L/b = 10$ as a function of Ra* also in Table III. Figure 6(a) shows that the flow rate ratio, $\Delta\Psi/\Delta\Psi_0$, varies inversely proportional with the total height ratio for fixed Ra* value. The lines are interweaved and nearly invariant with the size of the aspect ratio L/b. The largest reduction of

Table II. Flow rates and maximum wall temperatures for the "base case" at $Ra^* = 10^3$ and several L/b

L/b	2.5	5.0	10	15
$\Delta\Psi_0$	27.2	52.2	102	150
$\theta_{w,max\,0}$	0.461	0.486	0.493	0.500

Table III. Flow rates and maximum wall temperatures for the "base case" at $L/b = 10$ and several Ra^*

Ra*	10^3	10^4	10^5
$\Delta\Psi_0$	102	250	539
$\theta_{w,max\,0}$	0.493	0.295	0.179

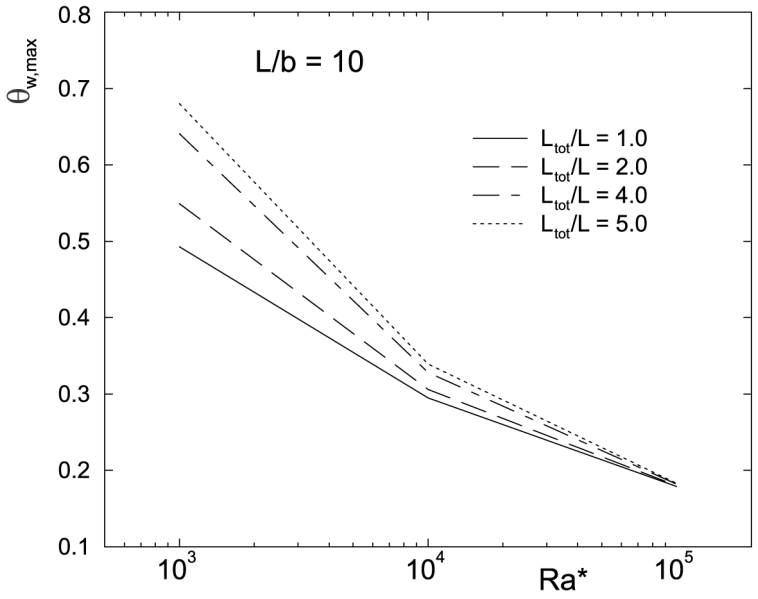

Figure 5.
Maximum wall temperatures as a function of Ra* at $L/b = 10$ for several L_{tot}/L

$\Delta\Psi/\Delta\Psi_0$ is about 40 per cent and is obtained for the highest L_{tot}/L considered, equal to 5.0. It is interesting that the maximum percentage difference is lower than 5 per cent for $L_{tot}/L = 4.0$. It can be concluded that for assigned Ra* value the dependence of $\Delta\Psi/\Delta\Psi_0$ on L/b is weak. In Figure 6(b), L/b is maintained fixed at 10, whereas the Ra* receives values of 10^3, 10^4 and 10^5. As Ra* increases, the lines move up gently showing a minor spread than the previous cases. For the specific value of Ra* $= 10^5$ the magnitude of $\Delta\Psi$ produces maximum wall temperature ratios, $\theta_{w,max}/\theta_{w,max\,0}$, which are connected to the base channel (Figure 4(b)). Thereby, it may be inferred that if Ra* is expanded to 10^6 there is an overlapping with the corresponding curves for Ra* $= 10^5$ in Figures 4(b) and 5(b) indicating the attainment of a "thermal saturation stage". This aspect suggests that the flow rate cannot be suppressed further, and as a result of this the wall temperature cannot increase further. When $L_{tot}/L = 5.0$ the $\Delta\Psi/\Delta\Psi_0$ percentage increase between the cases at Ra* $= 10^3$ and 10^4 is about 11 per cent, whereas comparing Ra* $= 10^4$ and 10^5 the increment is about 3 per cent.

The velocity profiles of the base channel (i.e. without extensions), are plotted at two locations: at the inlet plane, $X = 0$ and at the exit plane, $X = L/b$. Figure 7 shows the velocity curves for a fixed Ra*$=10^3$ and two different aspect ratio values $L/b = 2.5$ and 15 (Figure 7(a) and (c)). Here, some general trends are observed. The velocity profiles are flat at $X = 0$ and as the air accelerates the velocity profiles become more parabolic-wise at $X = L/b$. The magnitude of the velocities intensifies systematically with enlargements of L/b as a result of a stronger chimney effect. The velocity is susceptible to L/b: in fact, for case (a) $U_{max} = 35$ whereas for case (c) U_{max} is jacked up to 200. So, it is inferred that $U_{max} \approx 10 \times L/b$, approximately. The percentage increase of U_{max} between $X = 0.0$ and L/b is about 9.0 per cent and 12.5 per cent for $L/b = 2.5$ and 15, respectively. When $L_{tot}/L = 4.0$ is considered at Ra* $= 10^3$, the velocity

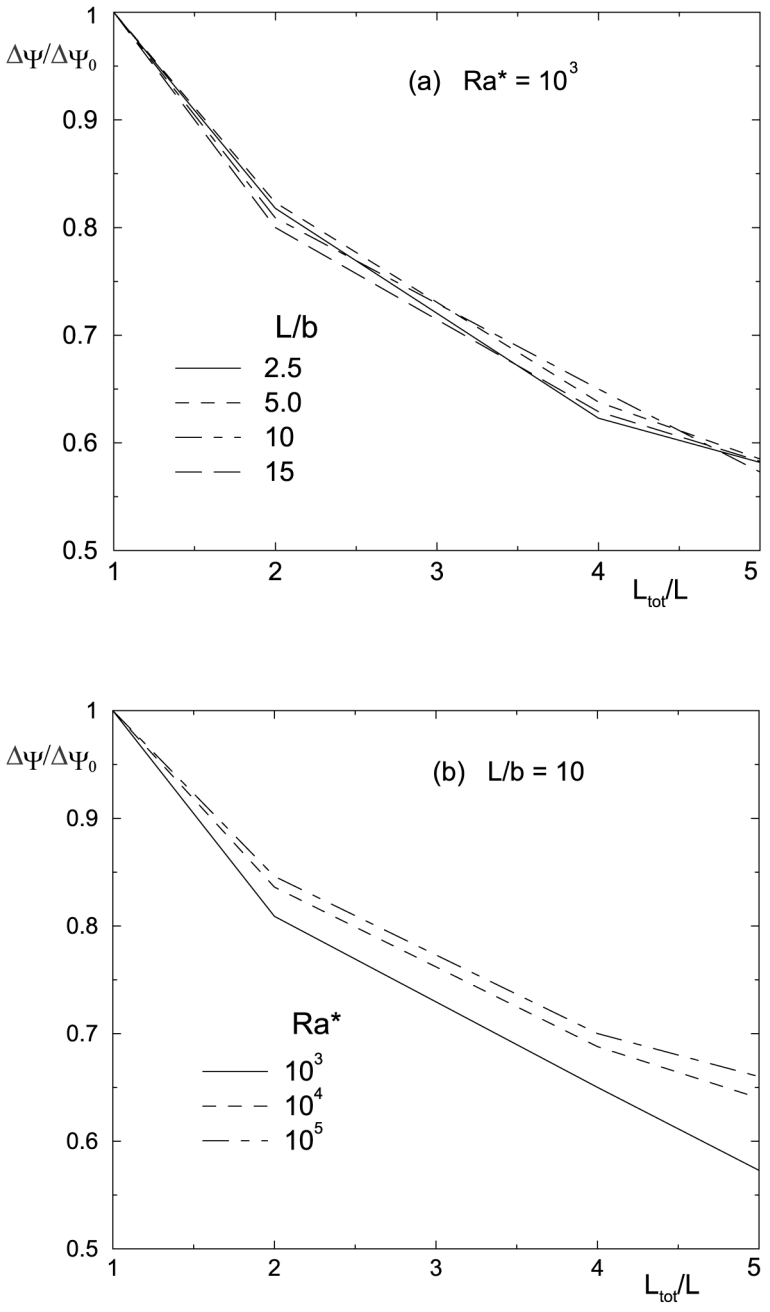

Figure 6.
Induced mass flow rate ratio as a function of L_{tot}/L for: (a) $Ra^* = 10^3$ and several L/b; and (b) $L/b = 10$ and several Ra^*

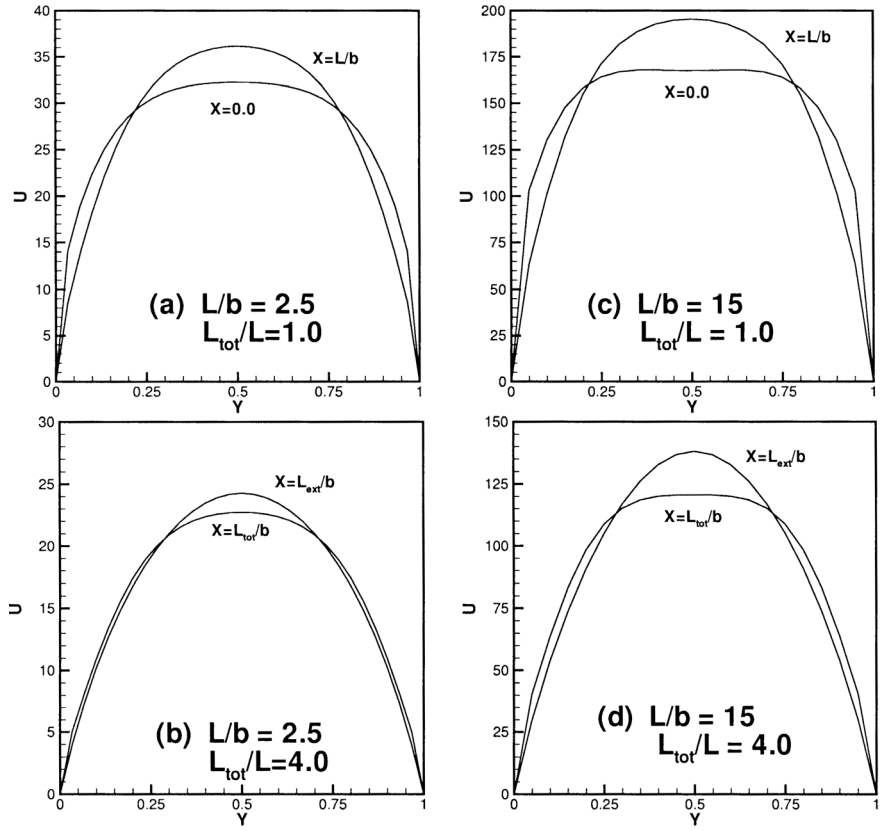

Figure 7.
Velocity profiles for $Ra^* = 10^3$

profiles plotted at $X = L_{ext}/b$ and $X = L_{tot}/b$ are shown in Figure 7(c) and (d), with $L/b = 2.5$ and 15. The thermal development modifies the hydrodynamic development of the buoyant flow, since the velocity profiles change their shape between the inlet and exit sections of the heated part. The fluid shows fully developed velocity profiles at the exit of the unheated part of the channel since it is three times the height of the heated part of the channel. When L/b is equal to 2.5 the maximum dimensionless velocity at the inlet of the heated part is 32 when $L_{tot}/L = 1.0$ and 24 when $L_{tot}/L = 4.0$, with a percentage reduction of about 25 per cent. This decrease is about 17 per cent when $L/b = 15$ and the maximum velocities are about 167 and 139 for $L_{tot}/L = 1.0$ and 4.0, respectively. However, percentage discrepancies between the maximum velocity for any configuration are lower than the case with $L_{tot}/L = 1.0$. Even if in this case the maximum velocity decreases between the inlet and exit section of the heated part. This can be due to the increase of the velocity close to the heated walls. The percentage decreases of U_{max} are about 7 per cent for $L/b = 2.5$ and 13 per cent for $L/b = 15$.

The temperatures profiles, for $Ra^* = 10^3$ and $L_{tot}/L = 1.0$ shown at X=0.0 and L/b, for L/b equal to 2.5 and 15, are shown in Figure 8(a) and (b). These profiles look like very similar and the temperatures at the exit are as high as L/b. In fact, the wall

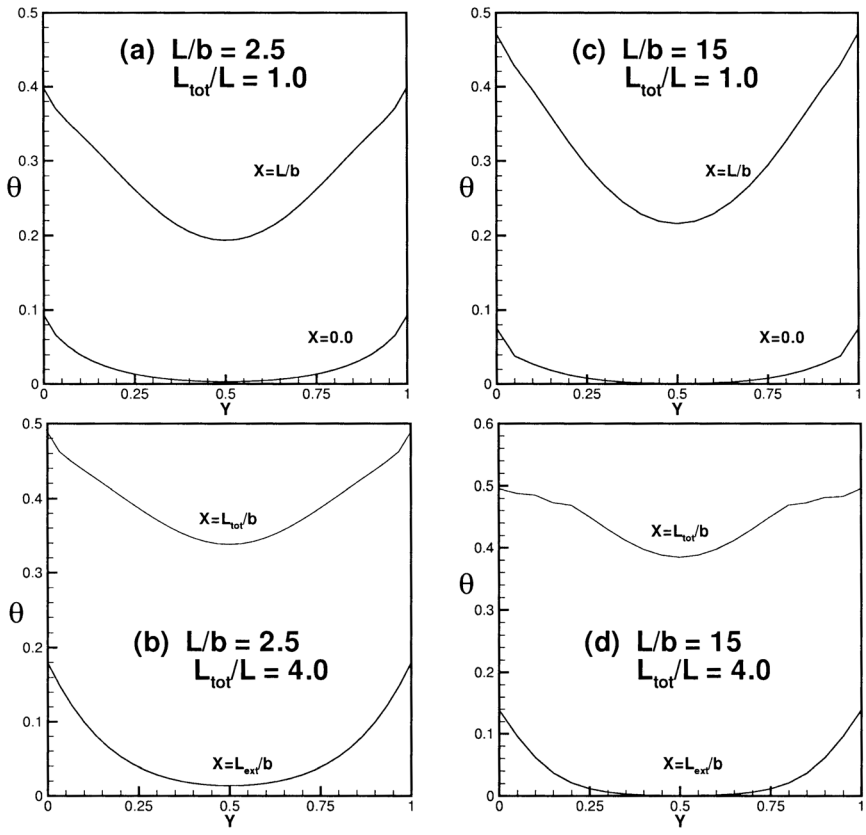

Figure 8.
Temperature profiles for Ra* = 10^3

temperature decrease of about 21 per cent at $X = 0.0$ comparing the case with $L/b = 2.5$ and 15. When $L/b = 2.5$ the thermal disturbance reaches the midplane of the section, whereas when $L/b = 15$ the temperature at $Y = 0.5$ is equal to the ambient one. At $X = L/b$ the temperature is higher at $L/b = 15$ than at $L/b = 2.5$. In fact, the wall values are 0.40 and 0.47 for $L/b = 2.5$ and 15, respectively. At the midplane section the values are 0.194 and 0.217 for $L/b = 2.5$ and respectively. The temperatures for $L_{tot}/L = 4.0$ and Ra* = 10^3 are shown in Figure 8(c) and (d) at $X = L_{ext}/b$ and L_{tot}/b for the same L/b of the previous figures. In these figures, the inlet sections of the heated part show temperature values greater than the corresponding previous cases, since the diffusive effects which preheat the fluid are more effective with the insulated extensions. In accordance with the reduction of the induced mass flow rate the temperatures attained at the heated part of the channel are always higher than the corresponding cases without extensions. In addition, the thermal development is more evident for larger values of L/b. The percentage increments of the wall temperatures are nearly the same at $X = 0.0$ and greater for $L/b = 2.5$, whereas at the midplane exit section they are greater for $L/b = 15$.

The velocity profiles at Ra* $= 10^3$ and 10^4, $L/b = 10$ and $L_{tot}/L = 1.0$ and 4.0 are shown in Figure 9. The profiles are presented at $X = 0.0$ and L_{ext}/b, when $L_{tot}/L = 1.0$, and $X = L_{ext}/b$ and L_{tot}/b for $L_{tot}/L = 4.0$. When $L_{tot}/L = 1.0$ (Figure 9(a)) the profiles are more hydrodynamically developed at Ra* $= 10^3$ than at Ra* $= 10^4$ (Figure 9(c)), and at this value the profile is flat at the inlet, due to the greater convective effects. On the other hand, the profile at Ra*$=10^4$ presents two maxima which are located at about $Y = 0.2$ and 0.8, at the channel exit. This trend means that at the higher Ra* value, the flow is developing and the height of the channel is no sufficiently high for the flow to become developed. This outcome is more noticeable for $L_{tot}/L = 4.0$ (Figure 9(b) and (d)) where the influence of the Ra* number can be observed. The profiles are shown at $X = L_{ext}/b$ and L_{tot}/b. The velocity profiles, which are developed at $X = L_{ext}/b$ modify their shape towards the channel exit, $X = L_{tot}/b$. At Ra* $= 10^4$ this change is more marked. These profiles present more pronounced maximum values than the case with $L_{tot}/L = 1.0$.

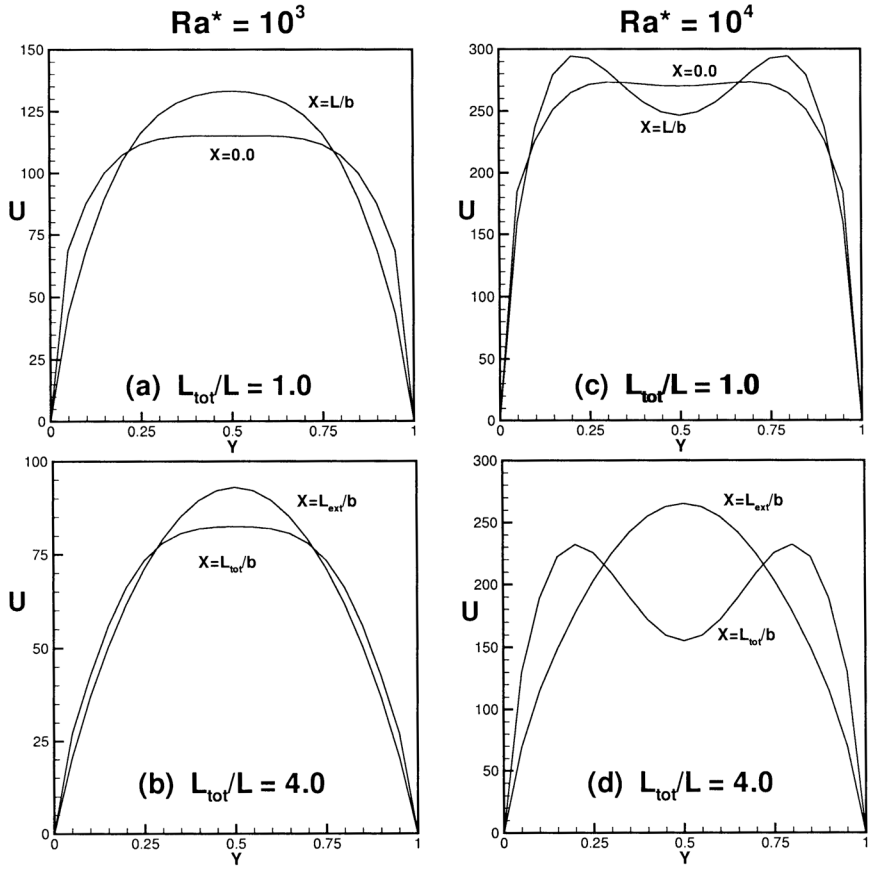

Figure 9.
Velocity profiles at Ra* $= 10^3$ and L/b=10

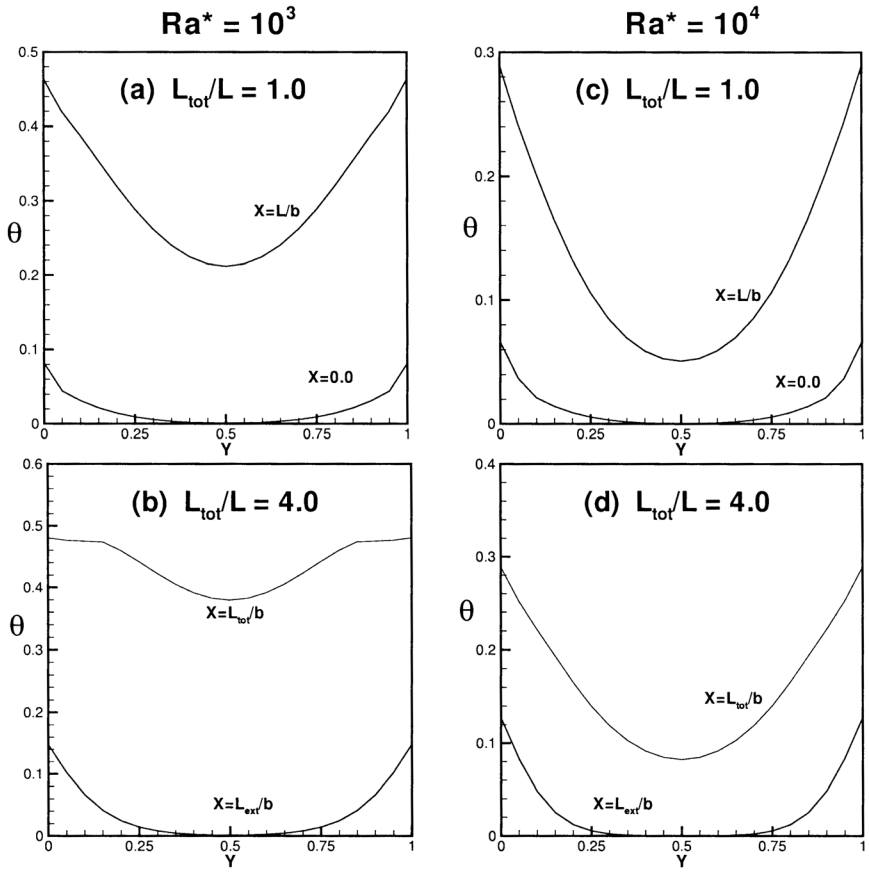

Figure 10.
Temperature profiles at $\mathrm{Ra}^* = 10^3$ and $L/b = 10$

The temperature profiles at $\mathrm{Ra}^* = 10^3$ and 10^4, and the same geometrical parameters of the previous figure are shown in Figure 10. When $L_{\mathrm{tot}}/L = 1.0$ (Figure 10(a) and (c)), the profiles at $X = 0.0$ show an undisturbed core in the central zone of the channel, indicating that the thermal diffusion was not able to preheat the core of the incoming fluid. Instead, at the channel exit, $X = L/b$, the profiles present a typical shape with a maximum located at the heated walls, and equal to 0.46 and 0.29 at $\mathrm{Ra}^* = 10^3$ and 10^4, respectively, and a minimum at the midplane whose values are 0.21 and 0.06, respectively. The case at $\mathrm{Ra}^* = 10^4$ shows a lower temperature value in the core zone than the case at $\mathrm{Ra}^* = 10^3$ because of the thinner thermal boundary layer thickness. The configurations with unheated extensions $L_{\mathrm{tot}}/L = 4.0$ (Figure 10(b) and (d)), present different patterns. In fact, the temperature values at $X = L_{\mathrm{tot}}/b$ are completely different for the two Ra* numbers because of the different velocity values in the heated part of the channel.

Next some correlation equations are proposed for the main interesting engineering quantities. The first one is the correlation equation of the induced mass flow rate $\Delta\Psi$

as function of the Ra*, the total extension ratio L_{tot}/L and the aspect ratio L/b. The equation reads:

$$\Delta\Psi = 0.951(\mathrm{Ra}^*)^{0.353}\left(\frac{L_{tot}}{L}\right)^{-0.287}\frac{L}{b} \tag{9}$$

with a regression coefficient $r^2 = 0.987$ and in the ranges: $10^3 \leq \mathrm{Ra}^* \leq 10^5$, and $1 \leq L_{tot}/L \leq 5$, $5 \leq L/b \leq 15$.

The other two correlation equations are for the average Nusselt number and the maximum wall temperature. They read, respectively:

$$\mathrm{Nu} = 0.773(\mathrm{Ra}^*)^{0.200}\left(\frac{L_{tot}}{L}\right)^{-0.0994} \tag{10}$$

$$\theta_{w,max} = 2.91(\mathrm{Ra}^*)^{-0.250}\left(\frac{L_{tot}}{L}\right)^{-0.116} \tag{11}$$

valid for the same range of parameters and with regression coefficients r^2 equal to 0.988 for both equations and in the ranges $10^3 \leq \mathrm{Ra}^* \leq 10^5$, $1 \leq L_{tot}/L \leq 5$, and $5 \leq L/b \leq 15$. By combining the equations (9) and (11) one can obtain the useful correlation equations which directly relate the maximum wall temperature as function of the induced mass flow rate and the average Nusselt number, the channel aspect ratio and the total extension ratio:

$$\theta_{w,max} = 2.81\left(\Delta\Psi\frac{b}{L}\right)^{-0.708}\left(\frac{L_{tot}}{L}\right)^{-0.0873} \tag{12}$$

$$\mathrm{Nu} = 0.796\left(\Delta\Psi\frac{b}{L}\right)^{0.566}\left(\frac{L_{tot}}{L}\right)^{0.0632} \tag{13}$$

It should be observed that in equation (9) there is a strong dependence of the induced flow rate on the total extension ratio L_{tot}/L, and even a stronger dependence on the channel aspect ratio L/b. As already observed in Campo *et al.* (1999), the dependence of the maximum wall temperature on the L_{tot}/L is quite weak and the same happens for the average Nusselt number.

Conclusions

The effects of two insulated plate extensions placed upstream of uniformly heated vertical channels were numerically investigated in terms of the controlling thermal and geometrical parameters, such as the channel Rayleigh number, Ra*, the total height ratio, L_{tot}/L, and the channel aspect ratio, L/b. The main results of practical interest that were derived from the investigation were the maximum wall temperatures, the induced mass flow rates as well as velocity and temperature profiles.

It was observed that the wall temperatures were less influenced by L/b than by L_{tot}/L (for fixed L/b) while more significant changes were found for different Ra* values ($10^3 \leq \mathrm{Ra}^* \leq 10^5$). The percentage of maximum wall temperature increments, due to

the reduction of the chimney effect, is of order 30 per cent when L/b is in the range 2.5-15 and $Ra^* = 10^3$, with $L_{tot}/L = 5.0$. The increment of the maximum wall temperature at the highest investigated Ra* value was lower than 4 per cent when $L_{tot}/L \leq 5.0$. The induced mass flow rate decreased with increasing L_{tot}/L and this decrement was heavily influenced by Ra*.

The velocity and temperature profiles supplied interesting observations in terms of local behaviour in the heated part of the channel. When $Ra^* = 10^3$ the adiabatic extensions, $L_{tot}/L = 4.0$, cause the velocity profile to be fully developed at the heated inlet section for any L/b. These profiles modified inside the heated part of the channel due to the thermal development. This effect was more relevant at higher Ra* values.

In addition, correlation equations for some important engineering quantities, such as the induced mass flow rate, the average Nusselt number and the maximum wall temperature, were proposed in terms of the channel Rayleigh number and geometrical parameters, L_{tot}/L and L/b in the following ranges: $10^3 \leq Ra^* \leq 10^5$, $1 \leq L_{tot}/L \leq 5$, and $5 \leq L/b \leq 15$.

References

Aihara, T. (1973), "Effects of inlet boundary condition on numerical solution of free convection between vertical parallel plates", *Rep. Inst. High-speed Mechanics*, Vol. 28, pp. 1-27.

Bergles, A.E. (1998), *Handbook of Heat Transfer – Fundamentals*, chapter 3, 3rd ed., McGraw-Hill, New York, NY.

Chang, B. and Lin, K. (1989), "Transient buoyancy-induced flow through a heated, vertical channel of finite height", *Numerical Heat Transfer, Part A*, Vol. 16, pp. 15-35.

Chang, B. and Lin, K. (1990), "On the reversed flow and oscillating wake in an asymmetrically heated channel", *Internationl Journal of Numerical Methods in Fluids*, Vol. 10, pp. 443-59.

Campo, A., Manca, O. and Morrone, B. (1996), "Numerical simulation of free convection heat transfer from localized discrete heat sources in a vertical channel", *ASME-HTD*, Vol. 333, pp. 275-86.

Campo, A., Manca, O. and Morrone, B. (1999), "Analysis of partially heated vertical parallel plates in natural convective cooling", *Numerical Heat Transfer, Part A*, Vol. 36, pp. 129-51.

Gebhart, B., Jaluria, Y., Mahajan, R. and Sammakia, B. (1988), *Buoyancy-Induced Flows and Transport*, Hemisphere, New York, NY, pp. 27-8.

Kettleborough, C.F. (1972), "Transient laminar free convection between heated vertical plates including entrance effects", *International Journal of Heat & Mass Transfer*, Vol. 15, pp. 883-96.

Lee, K.T. (1994), "Natural convection in vertical parallel plates with an unheated entry or unheated exit", *Numerical Heat Transfer, Part A*, Vol. 25, pp. 477-93.

Manca, O., Morrone, B. and Naso, V. (1994), "A numerical study of natural convection between symmetrically heated vertical parallel plates", *Atti del XII Congresso Nazionale sulla Trasmissione del Calore*, L'Aquila, Italy, UIT, pp. 379-90.

Manca, O., Morrone, B., Nardini, S. and Naso, V. (2000), *Computational Analysis of Convection Heat Transfer*, Chapter 7, WIT Press, Southampton, GB.

Martin, L., Raithby, G.D. and Yovanovich, M.M. (1991), "On the low Rayleigh number asymptote for natural convection through an isothermal, parallel-plate channel", *ASME Journal of Heat Transfer*, Vol. 113, pp. 899-905.

Morrone, B., Campo, A. and Manca, O. (1997), "Optimum plate separation in a vertical parallel-plate channel for natural convection flows: incorporation of large spaces at the channel extremes", *International Journal of Heat & Mass Transfer*, Vol. 40, pp. 993-1000.

Nakamura, H., Asako, Y. and Naitou, T. (1982), "Heat transfer by free convection between two parallel flat plates", *Numerical Heat Transfer*, Vol. 5, pp. 95-106.

Naylor, D., Floryan, J.M. and Tarasuk, J.D. (1991), "A numerical study of developing free convection between isothermal vertical plates", *ASME Journal of Heat Transfer*, Vol. 113, pp. 620-6.

Raithby, G.D. and Hollands, K.G.T. (1998), *Handbook of Heat Transfer*, Chapter 4, 3rd ed., McGraw-Hill, New York, NY.

Ramanahtan, S. and Kumar, R. (1991), "Correlations for natural convection between heated vertical plates", *ASME Journal of Heat Transfer*, Vol. 113, pp. 97-107.

Roache, J.P. (1972), *Computational Fluid Dynamics*, Hermosa publ., Albuquerque, NM.

Roache, J.P. (1998), *Verification and Validation in Computational Science and Engineering*, Hermosa publ., Albuquerque, NM.

Shyy, W., Gingrich, W.K. and Gebhart, B. (1992), "Adaptive grid solution for buoyancy-induced flow in vertical slots", *Numerical Heat Transfer, Part A*, Vol. 22, pp. 51-70.

Sparrow, E.M., Shah, S. and Prakash, C. (1980), "Enhancement of natural convection heat transfer by a staggered array of discrete vertical plates", *ASME Journal of Heat Transfer*, Vol. 102, pp. 215-19.

Torrance, K.E. (1985), *Handbook of Heat Transfer – Fundamentals*, Chapter 5, 2nd ed., McGraw-Hill, New York, NY.

Webb, R. (1994), *Principles of Enhanced Heat Transfer*, Wiley, New York, NY.

Wirtz, R.A. and Haag, T. (1985), "Effect of unheated entry on natural convection between vertical parallel plates", *ASME paper 85-WA/HT-14*, Miami Beach, ASME.